Nano Energy 43 (2018) 72–80

Contents lists available at ScienceDirect

Nano Energy

journal homepage: www.elsevier.com/locate/nanoen

Full paper

Reduced interface losses in inverted perovskite solar cells by using a simple dual-functional phenanthroline derivative

Zhao Hu[a], Jingsheng Miao[a], Tingting Li[a], Ming Liu[a], Imran Murtaza[b], Hong Meng[a,b,*]

[a] School of Advanced Materials, Peking University Shenzhen Graduate School, Shenzhen 518055, China
[b] Institute of Advanced Materials (IAM), Nanjing Tech University (Nanjing Tech), 5 Xinmofan Road, Nanjing 210009, China

ARTICLE INFO

Keywords:
Interface losses
Interface materials
Inverted perovskite solar cells

ABSTRACT

Interface losses at metal/organic interface is a critical issue in organic electronic devices. The interfacial layers play a significant role in enhancing the device performance and the interfacial material design criteria are ongoing challenges to be faced in optimization the device performance. In this work, a simple Phenanthroline derivative Phen-I was synthesized through a quaternization reaction in a high yield without complicated purification process. Besides its good wettability and compatibility of the contact between metal electrode and organic layer, interestingly, Phen-I displays a dual functional property, i.e., it not only lowers the work function of the metallic cathode to increase electron extraction but also can be doped into electron transporting material to enhance the conductivity. The inverted perovskite solar cells (PSCs) with Phen-I as cathode interlayer (CIL) show superior performance both in power conversion efficiency, with a maximum PCE of 18.13%, and devices stability as compared with the control devices. Encouragingly, the best PCE of 19.27% was obtained when the perovskite layer based on $FA_{0.3}MA_{0.7}PbI_{2.7}Cl_{0.3}$ perovskite system. Meanwhile, the devices with Phen-I as CIL show low *J-V* hysteresis during the forward and reverse bias sweeping. Subsequent studies demonstrate that the performance of the inverted PSCs also improves to 15.25% using 5% Phen-I:$PC_{61}BM$ as electron transporting layer (ETL). Herein, the interface between the metal electrode and ETL is carefully investigated using a series of electrical and surface potential techniques. These results demonstrate that Phen-I is a dual-functional interlayer material to reduce interface losses, which, highlights the broad promise of this new class of materials for applications in organic electronic devices. Meanwhile, owing to the simple molecular structure, low-cost and solution processible, these intriguing features render Phen-I more suitable for efficient organic electronics in large area printing process.

1. Introduction

Organic electronic devices, for example, organic light-emitting diodes (OLED) [1], organic thin film transistors (OTFT) [2,3], organic/inorganic hybrid photovoltaic [4–6], have recently attracted significant attention due to their high mechanical flexibility [7] and low fabrication cost [8,9] with a variety of choices available for material selection to improve the device performance. However, a critical issue for organic semiconductor devices, in general, is the interface losses at their electrode/organic interfaces [10]. Excellent charge injection leads to a lower turn-on voltage and higher efficiency in OLEDs [11,12], smaller contact resistance in OTFT [13] and a higher short-circuit current and open-circuit voltage in solar cells [14–17]. Interface modification has been considered as an effective approach for fine-tuning the device performance due to its abilities to tune the energy level alignment, surface energy and recombination induced by surface states and/or imperfections [18,19]. On the other hand, although the power conversion efficiency (PCE) of inverted PSCs has exceeded 20% [20,21], interface issue still need to resolved [22], where a low work function metal is normally needed to match with the LUMO energy level of electron transporting layer (ETL), in which PCBM commonly used as ETL material due to its solution processability, high electron mobility and fine energy levels for efficient excitons dissociation. Therefore, interface engineering is of paramount importance for improving the performance of organic electronic devices.

Recently, an effective approach has been carried out to reduce interface losses by incorporating a cathode interlayer between organic layer and metal electrode [23]. Thermally evaporated Ga, LiF [24], bathocuroine (BCP) [25], or functionalized fullerene derivatives [26] have been reported as interfacial layer in inverted PSCs. Meanwhile, Some solution processed materials, for example, conjugated polyelectrolytes [27,28], thiol-functional cation surfactant [29], n-doped metal

* Corresponding author at: School of Advanced Materials, Peking University Shenzhen Graduate School, Shenzhen 518055, China.
E-mail address: menghong@pkusz.edu.cn (H. Meng).

https://doi.org/10.1016/j.nanoen.2017.11.014
Received 4 August 2017; Received in revised form 27 September 2017; Accepted 6 November 2017
Available online 08 November 2017
2211-2855/ © 2017 Elsevier Ltd. All rights reserved.

oxides [30], amino-functionalized polymer (PN4N) [31], amino-functionalized small molecules (C_{60}-N [32], PDINO [10]), and carboxylic potassium salt [33] were also employed as an efficient interlayer to modify the interface between the PCBM and top metal contact. The Bis-C_{60} was already demonstrated to be a high efficient interfacial material [34,35] although its synthesis is complicated with relatively long synthetic routes [36]. In addition, Liao et al. reported costly Phen derivative 4,7-diphenyl-1,10-phenanthroline (Bphen) as CIL to modify the surface morphology of perovskite/PCBM and improve the performance of the devices [37]. Zou et al. introduced Bphen doped with bis(2-methyldibenzo-[*f*,*h*]quinoxaline) (Ir(MDQ)2(acac)) as CIL [38]. However, either a high vacuum-based expensive film deposition process or intricate expensive materials are required to fabricate the devices, which hinder the affordable use of the interfacial layer in printed and large-area devices. Here, we report a simple Phen derivative Phen-I, which was synthesized in one-step, using low-cost Phen as starting material and through a simple quaternization reaction with a high yield and without complicated purification process, for instance, costly chromatographic separations or tedious recrystallization process. The crude product was purified by simple washing with petroleum ether to afford a pure yellow solid. We demonstrated that high-performance inverted PSCs can be fabricated with Phen-I as an interlayer between $PC_{61}BM$ and silver electrode, achieving a maximum PCE of 18.13%. It has been demonstrated in a previous report that DMOAP can cause efficient n-doping of PCBM and achieve a high PCE of 18.1% [39]. However, DMOAP is highly unstable in air, which limits its further industrial application [40]. Interestingly, we found Phen-I could also n-dope $PC_{61}BM$ at the interface. The device performance with the Phen-I-doped $PC_{61}BM$ layer was then studied. In the case of 5 wt% Phen-I, the device demonstrated the best performance with a PCE of 15.25%, which is more than 42% increase compared with that of the control device. Kelvin probe force microscopy (KPFM), ESR spectroscopy, conductive atomic force microscopy (*c*-AFM) and steady-state photoluminescence (PL) were utilized to fully understand the influence of interface layer on the organic electronic device performance.

2. Material and methods

2.1. Synthesis of Phen-I

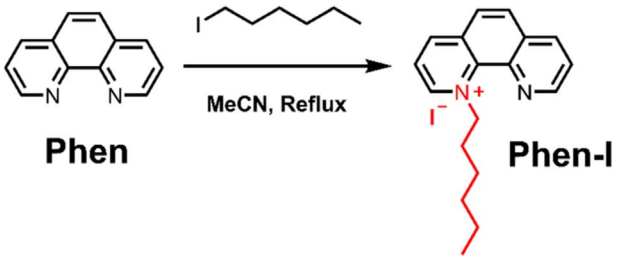

A nitrogen flushed round bottom flask was charged with Phen (1.8 g, 10 mmol), 1-iodohexane (2.3 g, 11 mmol). Acetonitrile (50 ml) was then added and the mixture was bubbled with nitrogen for 15 min. The mixture was then refluxed for 12 h. After removal of solvent, the crude product was purified by washing with petroleum ether for several times to afford a yellow solid (3.49 g, 89%). ^{1}H NMR ($CDCl_3$, 300 MHz): δ 10.20 (d, J=5.9 Hz, 1H), 9.44 (d, J=8.2 Hz, 1H), 9.22 (dd, J=4.3, 1.8 Hz, 1H), 8.49 (dd, J=8.2, 5.9 Hz, 1H), 8.36 (d, J=8.8 Hz, 1H), 8.26 (d, J=8.8 Hz, 1H), 7.92 (dd, J=8.2, 4.2 Hz, 1H), 6.19-6.02 (m, 2H), 2.21-2.03 (m, 2H), 1.59 (p, J=7.3 Hz, 2H), 1.44-1.21 (m, 3H), 0.86 (t, J=7.0 Hz, 3H). ^{13}C NMR (CDCl3, 300 MHz): δ 151.12, 149.76, 147.00, 139.88, 137.85, 136.58, 132.72, 132.06, 131.04, 127.34, 125.36, 125.09, 64.62, 31.82, 31.17, 25.89, 22.39, 13.92.

2.2. Materials characterization

Nuclear magnetic resonance (NMR) was taken on Bruker AVANCE III 300 MHz and 400 MHz Spectrometer. All chemical shifts were reported relative to tetramethylsilane (TMS) at 0.0 ppm, unless otherwise stated. The absorption spectrum was recorded with UV–visible spectrophotometer (Shimadzu 2450). Cyclic voltammetry was determined by electrochemical workstation (Chenhua CHI600E).

2.3. Device fabrication

2.3.1. Solar cell fabrication and testing

NiOx thin films were prepared according to the literature. The perovskite precursor solution was prepared by mixing FAI, CsI, MAI, PbI_2 and $PbCl_2$ with molar ratio of 0.1:0.1:0.8:0.9:0.1 in γ-GBL:DMSO=7:3 (v/v) at 1.4 mol/L and stirred at 60 °C for 6 h before using. Here, sequence three step spin coating process was applied to fabricate highly uniform perovskite thin films. In brief, the perovskite precursor solution was spin-coated on to the ITO/NiO_x substrates at 1000r/min and 5000r/min for 10 s and 30 s, at the 5000r/min for 20 s, toluene was used to treat the perovskite thin film. Then the perovskite thin films were thermal annealing on the hot plate at 100 °C for 10 min. The inverted PSCs based on $FA_{0.3}MA_{0.7}PbI_{2.7}Cl_{0.3}$ perovskite system was fabricated according to the literature.[39] For $PC_{61}BM$ layer, 10 mg/ml $PC_{61}BM$ chloroform solution (doped 0%, 2%, 5% and 10% with Phen-I) was spin-coated onto the perovskite layer. For device with Phen-I as cathode interlayer, 2 mg/ml Phen-I methanol solution was pin-coated onto the $PC_{61}BM$ layer for 30 s at 2000r/min. Lastly, a 90 nm Ag film was evaporated through a shadow mask in a vacuum chamber under a pressure of 1×10^{-4} Pa. The device area was 0.045 cm^2.

2.3.2. Device characterization

The *J-V* characteristics of devices were recorded by a Keithley 2400 source-measurement unit under simulated AM 1.5 G (100 mW/cm^2) spectrum (Newport, Oriel AM 1.5G, 100 mW/cm^2). The light intensity was calibrated by an NREL-certified monocrystalline Si diode. The EQE spectrum was measured by EQE measurement system (Enlitech, Inc.).

The contact potential differences between the AFM probe and bare Ag electrode or Ag/Phen-I were recorded by a MultiMode 8-HR AFM (Bruker Corporation, Germany). The conductivities of Phen-I can dope $PC_{61}BM$ thin film was measured by this AFM equipment too. The ESR spectroscopy of $PC_{61}BM$/Phen-I blended sample was measured by an EMX^{plus}-10/12 Electron Paramagnetic Resonance Spectrometer (Bruker Corporation, Germany). Steady state PL spectra of the Perovskite films with and without $PC_{61}BM$ were measured by FLS920 spectrofluorimeter (Edinburgh Instruments).

3. Results and discussions

The photophysical and electrochemical properties of Phen-I are summarized in Table S1 (in Supporting information), and the corresponding UV–*vis* absorption spectra are shown in Fig. 1a. Cyclic voltammetry (CV) measurements were used to measure the electronic energy levels of Phen-I. The LUMO energy levels were calculated from the onset reduction potential by assuming the energy level of ferrocene/ferrocenium (Fc/Fc^+) to be −4.8 eV below the vacuum level. Fig. 1b displays the cyclic voltammograms of Phen-I in Bu_4NPF_6 (0.1 M in acetonitrile) solution at a scan rate of 100 mV s^{-1}. The onset reduction potentials of Phen-I is −1.18 eV (vs. Fc/Fc^+). Therefore, the LUMO energy level was calculated accordingly as −3.62 eV for Phen-I. The HOMO energy level of Phen-I was calculated from its LUMO level and optical band gap based on the equation of HOMO=LUMO-E_g. From 1a, the absorption edge of Phen-I is 473 nm, which correspond to the optical E_g of 2.62 eV. Hence, the calculated HOMO energy levels as shown in Fig. 4d, and the deep HOMO energy levels provide good hole

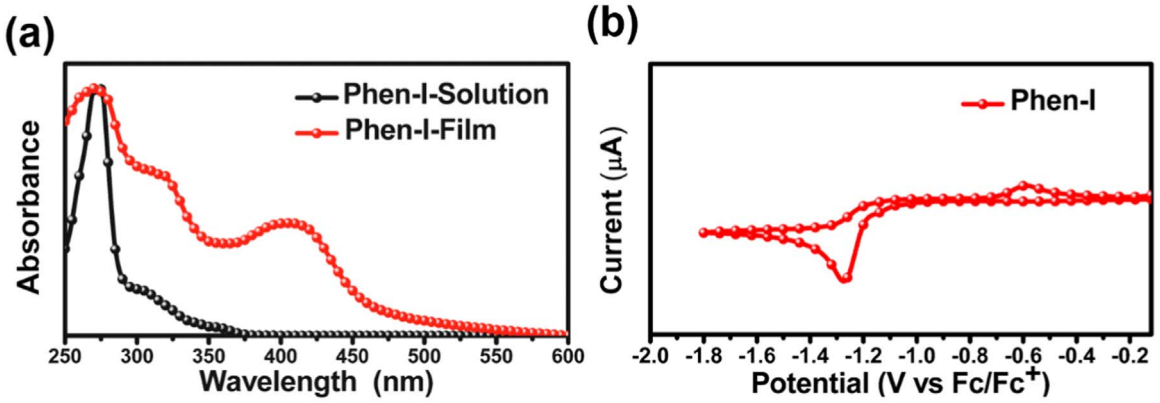

Fig. 1. a) Uv–*vis* spectra of Phen-I in solution and thin film. b) Cyclic voltammograms of Phen-I.

blocking ability to prevent undesired charges reaching the cathode, which reduces hole-electron recombination at the cathode interface.

To examine the performance of inverted PSCs with Phen-I as CIL, we fabricated the inverted PSCs with the configuration of ITO/NiO_x/Perovskite layer/$PC_{61}BM$/CIL/Ag as shown in Fig. 2a. The CIL was prepared by spin-coating the methanol solution of Phen-I on the $PC_{61}BM$ layer. Control devices without CIL were also fabricated. The current density-voltage (*J-V*) characteristics of the optimized devices under illumination of AM 1.5G, 100 mW/cm^2 are shown in Fig. 2b and corresponding photovoltaic parameters of the devices are summarized in Table 1. It is obvious that devices with Phen-I as CIL show higher PCEs, which indicates that Phen-I is an effective choice to modify the cathode interface. With Phen-I as the CIL, the inverted PSCs exhibit the best PCE of 18.13%, a V_{oc} of 1.13 V, a J_{sc} of 20.51 mA/cm^2, and FF of 78.54%. The best Phen-I device shows a PCE value as high as 18.13%, while the control device showed only the best PCE of 10.7%, with V_{oc} of 1.10 V, a J_{sc} of 18.15 mA/cm^2, and FF of 53.56%, the improvement in

Table 1
Photovoltaic parameters of PSCs with different cathode configurations.

Cathode configuration	V_{oc} (V)	J_{sc}(mA/cm^2)	*FF* (%)	*PCE* (%)
$PC_{61}BM$/Ag	1.10	18.15	53.56	10.70
$PC_{61}BM$/Phen-I/Ag	1.13	20.51	78.54	18.13

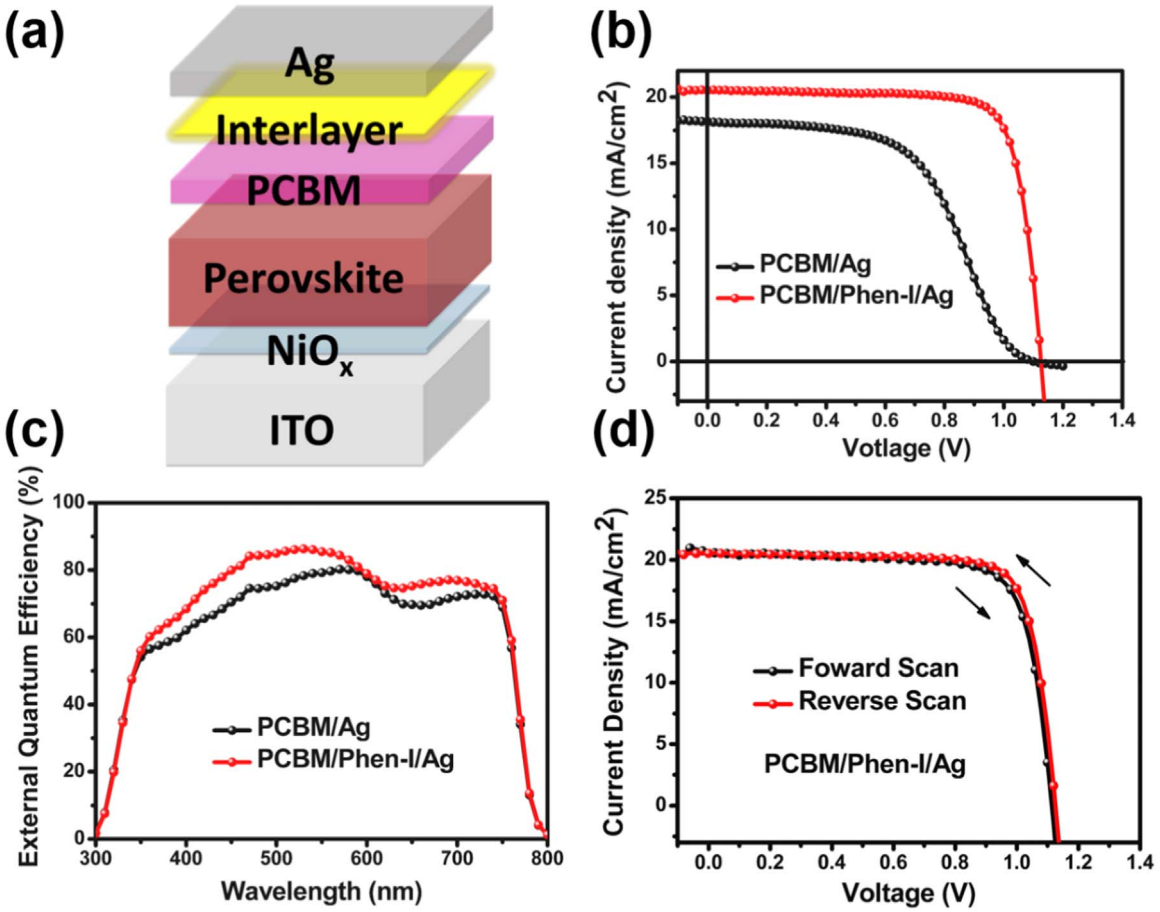

Fig. 2. a) Device configuration of the inverted PSCs with Phen-I as CIL. b) *J-V* curves of the devices with Phen-I and $PC_{61}BM$ as CIL, as measured under 100 mW/cm^2 Am 1.5G irradiation. c) EQE spectra of the corresponding solar cells. d) Hysteresis investigation of the device with Phen-I as CIL.

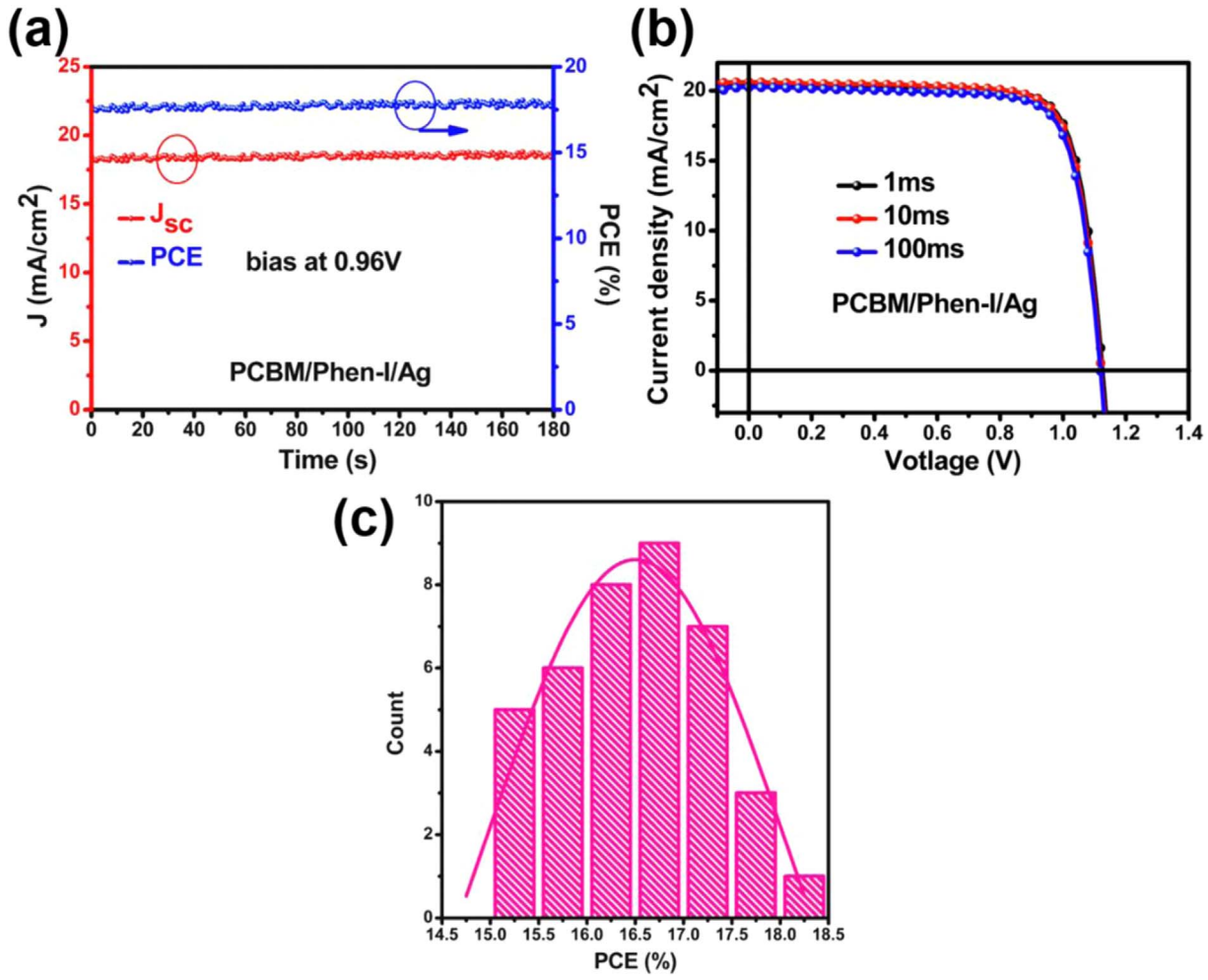

Fig. 3. a) Stable output power efficiency and photocurrent density biased near the maximum power point of the studied inverted PSCs, as measured under 100 mW/cm^2 AM 1.5G irradiation. b) *J-V* curves of inverted PSCs devices with pure PCBM or Phen-I:$PC_{61}BM$ ETL measured under 100 mW/cm^2 Am 1.5G irradiation. c) PCE histogram of 30 devices containing Phen-I interlayer.

the performance of Phen-I device is attributed to higher J_{sc} and FF. Fig. 2c shows the external quantum efficiency (EQE) measurement which was applied to confirm the higher J_{sc} of device with Phen-I as CIL. Obviously, the EQE values in the entire photo response range between 300 nm and 750 nm are significantly enhanced after inserting the CIL, suggesting that electrons can be more efficiently extracted from perovskite layer to Ag. The calculated J_{sc} from EQE measurement is well consistent with the measured J_{sc} value within 5% mismatch. Meanwhile, the devices with Phen-I as CIL show low *J-V* hysteresis (Fig. 2d) upon forward and reverse bias sweeping illustrating a negligible number of defects in the perovskite active layer and interfaces.

To confirm power output reliability of the fabricated PSCs with Phen-I as CIL, a stabilized power output was measured under a constant voltage bias of 0.96 V near the maximum power output point and is shown in Fig. 3a. The Phen-I device shows high stable power output and a steady-state PCE of 18.10% is obtained. The scan rate dependence of the *J-V* characteristics in the Phen-I-based device is given in Fig. 3b, and no significant change in the *J-V* characteristics was observed up to delay time of 100 ms. A histogram of the performance of Phen-I-based devices obtained from 30 samples is summarized in Fig. 3c. Notably, more than 50% of the integrated devices showed PCE above 16.7%, indicating good reproducibility. These results demonstrate that Phen-I is a promising CIL for inverted PSCs

In order to confirm a reduced injection barrier at $PC_{61}BM$/Ag by inserting Phen-I layer, we carried out Kelvin Probe Force Microscopy Measurement (KPFM) measurements to determine the contact potential differences (V_{CPD}) between the atomic force microscopy (AFM) probe and bare Ag electrode or Ag/Phen-I. The samples for KPFM were prepared by evaporating Ag onto a clean ITO glass, followed by spin-coating Phen-I from methanol. In a normal KPFM research work, firstly a pass scan is done in mechanically driven tapping mode to test topography, and then a second pass at AC voltage resonant frequency to determine V_{CPD}. Potential maps were showed in Fig. 4a and b. Potential histograms were made and fit with Gaussian curves to find the value of V_{CPD} for the sample. Representative V_{CPD} histograms for Ag electrode, Ag/Phen-I are shown in Fig. 4c. We found ΔV_{CPD} between bare Ag and Ag/Phen-I to be 0.18 ± 0.01. By the equation: $V_{CPD} = (\phi_{probe}\text{-}\phi_{sample})/\text{-}e$ we estimated a 0.18 eV ϕ decrease when Phen-I is coated on Ag. This apparent decrease in Ag ϕ arises from the presence of a negative interfacial dipole between Ag and Phen-I, and explains the improved V_{oc} for devices containing Phen-I interlayer [41].

Increased conductivity of electron transporting layer is important to enhance electron transport and collection by cathode [42]. Previous study has demonstrated that the iodide functional small molecule can n-dope fullerene films and increase its conductivity [43]. To confirm whether Phen-I can dope $PC_{61}BM$ thin film, electron spin resonance (ESR) spectroscopy was performed to further investigate the interface modification property. As shown in Fig. 5a, blended samples of $PC_{61}BM$/Phen-I with the 1:1 weight ratio were tested to study the charge transfer property between the two components. In the $PC_{61}BM$/Phen-I blend, an obvious resonance peak was detected. This result clearly suggests that electron transfer occurred from Phen-I to $PC_{61}BM$.

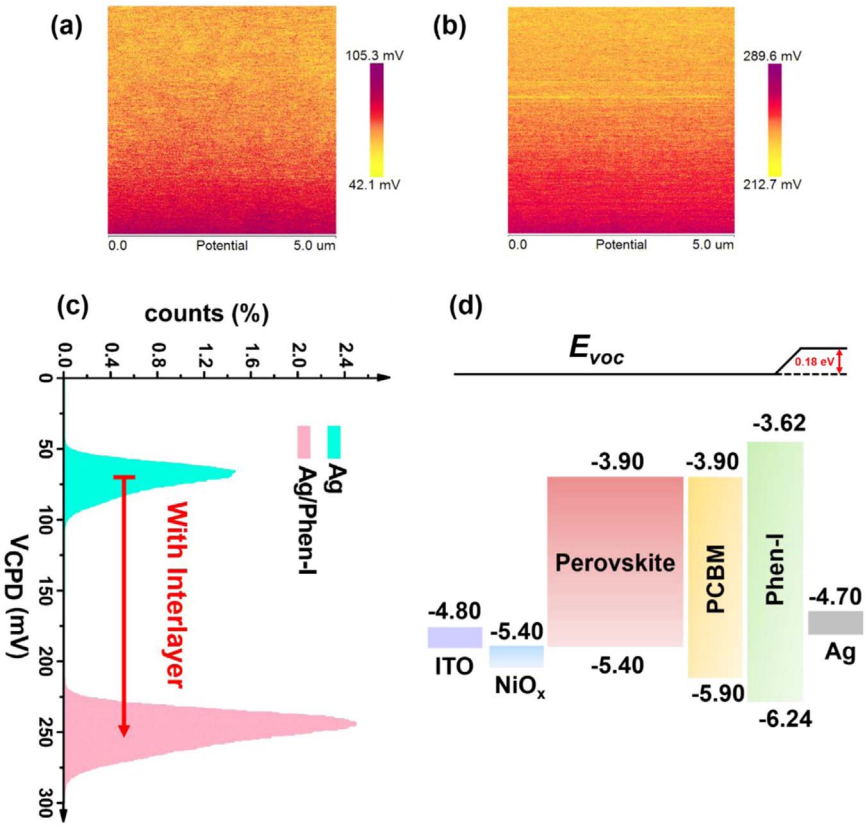

Fig. 4. Surface potential maps from KPFM measurements for a) bare Ag and b) Ag/Phen-I. c) Representative V_{CPD} histograms of surface potential maps. d) Energy level diagram of the device.

The results from the ESR study provide the evidence that Phen-I could n-dope $PC_{61}BM$ at the interface, leading to improve PSCs device performance. For investigation of the effect of Phen-I-doped $PC_{61}BM$ on the photovoltaic performance of PSCs, a configuration of glass substrate ITO/NiOx/Perovksite/Phen-I-doped $PC_{61}BM$/Ag was fabricated (Device configuration in Fig. 5b). Fig. 5c shows the *J-V* characteristics of the best performing devices, and the detailed photovoltaic parameters are listed in Table 2. There is a large effect of Phen-I concentration on the device performance. In the case of 5 wt% Phen-I, the device

Table 2
Photovoltaic parameters of PSCs with different ETL.

Cathode configuration	V_{oc} (V)	J_{sc}(mA/cm^2)	*FF* (%)	*PCE* (%)
PCBM/Ag	1.10	18.15	53.56	10.70
PCBM:Phen-I (10%)/Ag	1.01	19.67	64.79	12.93
PCBM:Phen-I (5%)/Ag	1.06	20.16	71.51	15.25
PCBM:Phen-I (2%)/Ag	1.06	19.20	66.70	13.63

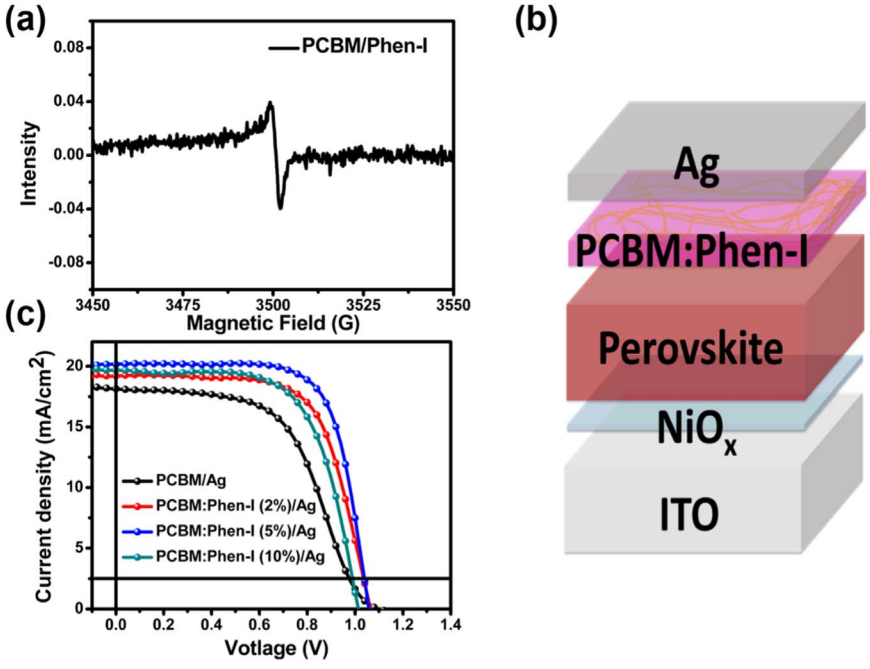

Fig. 5. a) ESP spectra of $PC_{61}BM$/Phen-I blend in solid state. b) Device configuration of the inverted PSCs with Phen-I:$PC_{61}BM$ as ETL. c) *J-V* curves of invert PSCs devices with pure $PC_{61}BM$ or Phen-I:$PC_{61}BM$ ETL measured under 100 mW/cm^2 Am 1.5G irradiation.

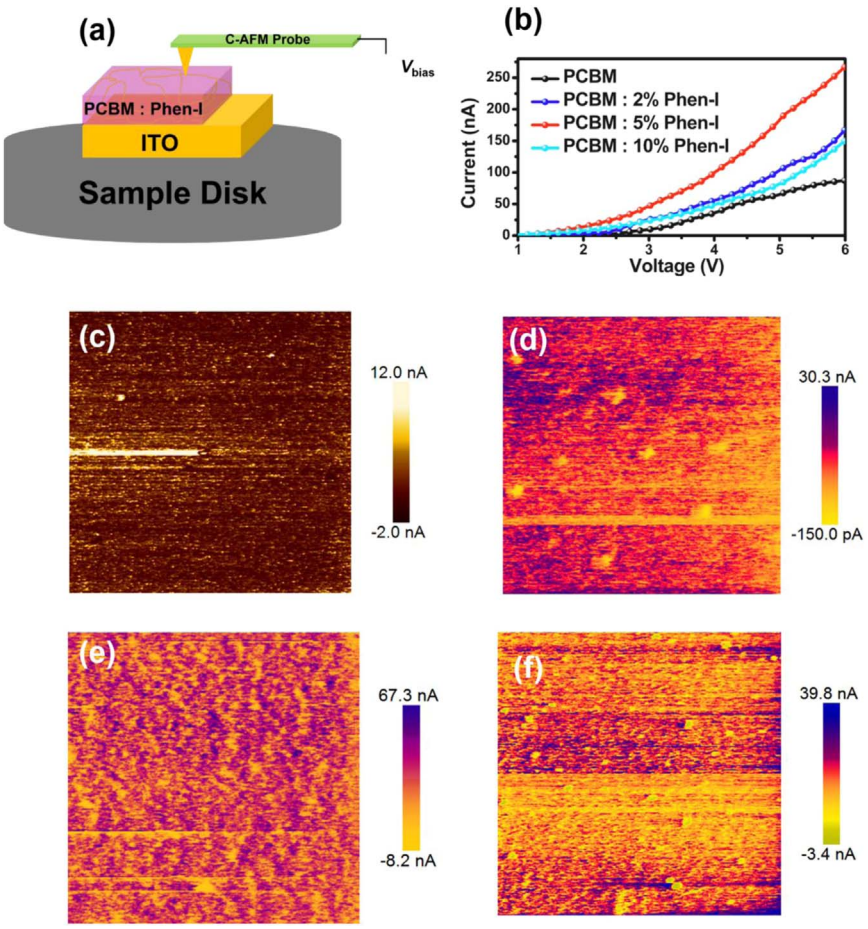

Fig. 6. a) Schematic diagram of c-AFM measurements. b) *I-V* curves of bare $PC_{61}BM$ and Phen-I: $PC_{61}BM$ measured by c-AFM. c-AFM images of c) bare NiOx, d) 2%Phen-I:$PC_{61}BM$, e) 5%Phen-I:$PC_{61}BM$, f) 10%Phen-I:$PC_{61}BM$.

demonstrated the best performance with a PCE of 15.25%, J_{sc} of 20.16 mA/cm^2, V_{oc} of 1.06V, and FF of 71.51%. It is found that the J_{sc} and FF in Phen-I-based cells improve largely in contrast to reference device. The J_{sc} increases from 18.15 to 20.16 mA/cm^2 and FF increases from 53.56% to 71.51%. Noticeably, the V_{oc} reduces slightly from 1.10 to 1.06 eV.

To investigate the effects of Phen-I-doping and device performance, we initially examined and compared the conductivity of $PC_{61}BM$ film with different doping concentrations by performing conductive atomic force microscopy (*c*-AFM) measurements as described in Fig. 6a. The *c*-AFM images in Fig. 6c, d, e, f clearly illustrate different current levels and distributions between bare $PC_{61}BM$ and Phen-I:$PC_{61}BM$ films. Obviously increased vertical current is found in the Phen-I:$PC_{61}BM$ films, demonstrating enhanced electrical conductivity upon Phen-I doping, which could attribute to anion-induced electron transfer [43]. The *I-V* curves presented in Fig. 6b also indicate the enhancement in electrical conductivity upon Phen-I doping as compared to bare $PC_{61}BM$. However, when the doping concentrations were increased beyond 5%, the conductivity decreased gradually which is consistent with the performance trend of PSCs. This deterioration could be ascribe to the tendency of excess Phen-I-caused aggregation [44]. Furthermore, the root-mean-square (RMS) roughness tests (Fig. S3) also indicate that higher doping concentration results in higher roughness.

To gain further insight into the charge transfer properties between Perovskite and $PC_{61}BM$, we performed steady-state photoluminescence (PL). The PL properties of ITO/Perovskite, TIO/Perovskite/$PC_{61}BM$, and TIO/Perovskite/Phen-I-doped $PC_{61}BM$ (doping concentration = 2, 5, 10 wt%) were measured under excitation at a wavelength of 450 nm. As shown in Fig. 7a, the significant PL quenching effect can be observed when the perovskite layer was deposited with either undoped $PC_{61}BM$ or doped $PC_{61}BM$ layers. The quenching of PL intensity is generally attributed to charge transfer at the perovskite/fullerene interface [45]. Compared with undoped $PC_{61}BM$-coated sample, nearly all intensities are quenched for the doped $PC_{61}BM$-coated sample (as shown in Fig. 7b), suggesting that charge carrier transfer at the perovskite/doped $PC_{61}BM$ interface is more efficient than that at the perovskite/undoped $PC_{61}BM$ interface, due to the higher electrical conductivity of doped $PC_{61}BM$ on the perovskite layer as discussed above.

In addition to the PCE, the stability is another important aspect that needs to be improved for the practical application of PSCs [46]. We investigated the stability of the devices with Phen-I as interlayer in the ambient conditions. We found that the insertion of the Phen-I layer is helpful to enhance the stability of the devices. As shown in Fig. 7c, the PCE of the devices without CBL drop rapidly. Merely 50% of the PCE remained after ≈ 200 h of storage in air. However, for the devices with CBL, the PCEs remained relatively stable even up to ≈ 300 h. After storing for 500 h in air, the PCEs still maintained 60% of the original PCE. These results illustrate that the Phen-I CIL may have a blocking effect on water and/or oxygen to some extent, which is greatly helpful to enhance the device stability.

It is worth mentioning that Phen-I was also successfully applied in other perovskite systems. We fabricated the inverted PSCs based on $FA_{0.3}MA_{0.7}PbI_{2.7}Cl_{0.3}$ perovskite system, which possesses a small bandgap. Encouragingly, the best PCE of 19.27% was obtained, with J_{sc} of 23.14 mA/cm^2, V_{oc} of 1.07 V, and *FF* of 77.98% (Fig. 8a) when Phen-I interlayer was incorporated. These results indicate that Phen-I can be used as a universal CIL for PSCs.

4. Conclusions

In conclusion, we synthesized a simple Phen derivative, Phen-I, and demonstrated a considerable enhancement in PCEs, from 10.70% to

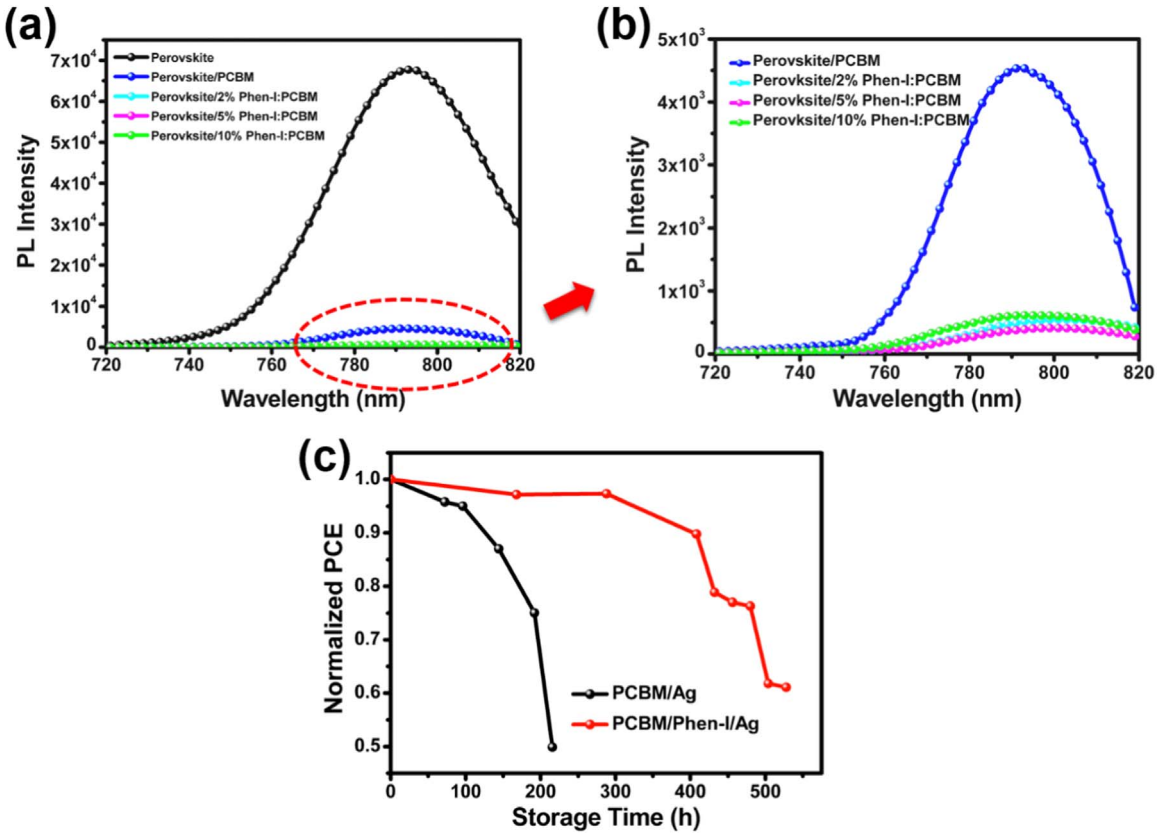

Fig. 7. a), b) Steady state PL spectra of the Perovskite films with and without $PC_{61}BM$, respectively. c) Stability investigation performed by storing six unencapsulated devices using Phen-I as interlayer in air and in the absence of light (the devices were stored at ambient atmosphere with a humidity of ≈ 30% and the devices were brought back into the glovebox for testing each time).

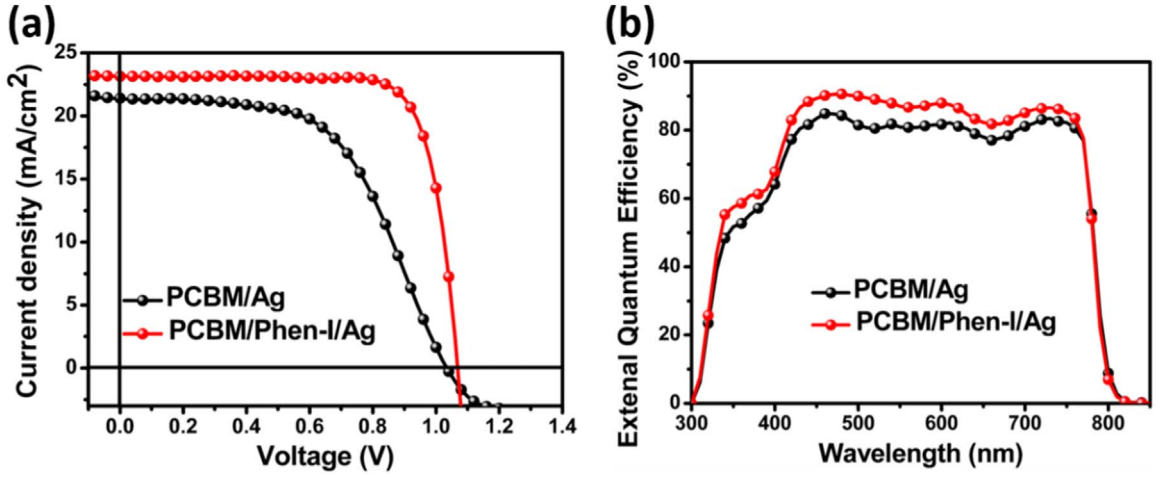

Fig. 8. a) J-V curves of the best performing $FA_{0.3}MA_{0.7}PbI_{2.7}Cl_{0.3}$-Based Devices under simulated AM 1.5 solar irradiation. b) EQE spectra of the corresponding solar cells.

18.13%, of inverted PSCs by inserting Phen-I as interlayer between metal electrode and ETL. The best PCE of 19.27% was obtained when the perovskite layer based on $FA_{0.3}MA_{0.7}PbI_{2.7}Cl_{0.3}$ perovskite system. Meanwhile, the performance of the inverted PSCs was also improved to 15.25% using 5% Phen-I:$PC_{61}BM$ as ETL. A variety of electrical and surface potential characterization measurements were used to study the interface between the metal electrode and ETL. KPFM measurements indicate a uniform and continuous work function decrease in the presence of the Phen-I layer. *c*-AFM measurements illustrate that the Phen-I-doping fully enhances the conductivity of PCBM film via anion-induced electron transfer. With the aid of these results we demonstrated Phen-I as a new dual-functional interlayer material to reduce interface losses for PSCs. Owing to the simple molecular structure and low-cost, Phen-I is also a good candidate for efficient organic electronics in large area printing process. The concept of such simple derivatives can be extended to explore new efficient interface materials.

Acknowledgements

We acknowledge the financial support from the Shenzhen Science and Technology Research Grant (JCYJ20160510144254604), National Basic Research Program of China (973 Program, No. 2015CB856505), Guangdong Academician Workstation, Shenzhen Science and Technology Research Grant (JCYJ20150629144328079, JCYJ20150331100628880),

Shenzhen Hong Kong Innovation Circle joint R & D project (SGLH20161212101631809) and the China (Shenzhen)-Israel Technology Collaboration Project (GJHZ20170313145720459).

Notes

The authors declare no competing financial interest.

Appendix A. Supporting information

Supplementary data associated with this article can be found in the online version at http://dx.doi.org/10.1016/j.nanoen.2017.11.014.

References

[1] C.W. Tang, S.A. VanSlyke, Organic electroluminescent diodes, Appl. Phys. Lett. 51 (12) (1987) 913–915.
[2] J. Mei, Y. Diao, A.L. Appleton, L. Fang, Z. Bao, Integrated materials design of organic semiconductors for field-effect transistors, J. Am. Chem. Soc. 135 (18) (2013) 6724–6746.
[3] L. Torsi, M. Magliulo, K. Manoli, G. Palazzo, Organic field-effect transistor sensors: a tutorial review, Chem. Soc. Rev. 42 (22) (2013) 8612–8628.
[4] M.A. Green, A. Ho-Baillie, H.J. Snaith, The emergence of perovskite solar cells, Nat. Photonics 8 (7) (2014) 506–514.
[5] A. Kojima, K. Teshima, Y. Shirai, T. Miyasaka, Organometal halide perovskites as visible-light sensitizers for photovoltaic cells, J. Am. Chem. Soc. 131 (17) (2009) 6050–6051.
[6] S. Shi, Y. Li, X. Li, H. Wang, Advancements in all-solid-state hybrid solar cells based on organometal halide perovskites, Mater. Horiz. 2 (4) (2015) 378–405.
[7] P. Docampo, J.M. Ball, M. Darwich, G.E. Eperon, H.J. Snaith, Efficient organometal trihalide perovskite planar-heterojunction solar cells on flexible polymer substrates, Nat. Commun. 4 (2013) 2761.
[8] A. Mei, X. Li, L. Liu, Z. Ku, T. Liu, Y. Rong, M. Xu, M. Hu, J. Chen, Y. Yang, M. Graetzel, H. Han, A hole-conductor-free, fully printable mesoscopic perovskite solar cell with high stability, Science 345 (6194) (2014) 295–298.
[9] M. Eslamian, Inorganic and organic solution-processed thin film devices, Nano-Micro Lett. 9 (1) (2016) 3.
[10] Y. Hou, W. Chen, D. Baran, T. Stubhan, N.A. Luechinger, B. Hartmeier, M. Richter, J. Min, S. Chen, C.O.R. Quiroz, N. Li, H. Zhang, T. Heumueller, G.J. Matt, A. Osvet, K. Forberich, Z.-G. Zhang, Y. Li, B. Winter, P. Schweizer, E. Spiecker, C.J. Brabec, Overcoming the interface losses in planar heterojunction perovskite-based solar cells, Adv. Mater. 28 (25) (2016) 5112–5120.
[11] C. Duan, L. Wang, K. Zhang, X. Guan, F. Huang, Conjugated zwitterionic polyelectrolytes and their neutral precursor as electron injection layer for high-performance polymer light-emitting diodes, Adv. Mater. 23 (14) (2011) 1665–1669.
[12] X. Guan, K. Zhang, F. Huang, G.C. Bazan, Y. Cao, Amino N-oxide functionalized conjugated polymers and their amino-functionalized precursors: new cathode interlayers for high-performance optoelectronic devices, Adv. Funct. Mater. 22 (13) (2012) 2846–2854.
[13] C.-a. Di, Y. Liu, G. Yu, D. Zhu, Interface engineering: an effective approach toward high-performance organic field-effect transistors, Acc. Chem. Res. 42 (10) (2009) 1573–1583.
[14] H.-L. Yip, A.K.Y. Jen, Recent advances in solution-processed interfacial materials for efficient and stable polymer solar cells, Energy Environ. Sci. 5 (3) (2012) 5994–6011.
[15] R. Fan, Y. Huang, L. Wang, L. Li, G. Zheng, H. Zhou, The progress of interface design in perovskite-based solar cells, Adv. Energy Mater. 6 (17) (2016) 1600460.
[16] C.-C. Chueh, C.-Z. Li, A.K.Y. Jen, Recent progress and perspective in solution-processed Interfacial materials for efficient and stable polymer and organometal perovskite solar cells, Energy Environ. Sci. 8 (4) (2015) 1160–1189.
[17] J. Shi, X. Xu, D. Li, Q. Meng, Interfaces in perovskite solar cells, Small 11 (21) (2015) 2472–2486.
[18] H. Kim, K.-G. Lim, T.-W. Lee, Planar heterojunction organometal halide perovskite solar cells: roles of interfacial layers, Energy Environ. Sci. 9 (1) (2016) 12–30.
[19] Y. Zhou, C. Fuentes-Hernandez, J. Shim, J. Meyer, A.J. Giordano, H. Li, P. Winget, T. Papadopoulos, H. Cheun, J. Kim, M. Fenoll, A. Dindar, W. Haske, E. Najafabadi, T.M. Khan, H. Sojoudi, S. Barlow, S. Graham, J.-L. Brédas, S.R. Marder, A. Kahn, B. Kippelen, A universal method to produce low–work function electrodes for organic electronics, Science 336 (6079) (2012) 327–332.
[20] F. Xie, C.-C. Chen, Y. Wu, X. Li, M. Cai, X. Liu, X. Yang, L. Han, Vertical recrystallization for highly efficient and stable formamidinium-based inverted-structure perovskite solar cells, Energy Environ. Sci. (2017), http://dx.doi.org/10.1039/C7EE01675A.
[21] X. Zheng, B. Chen, J. Dai, Y. Fang, Y. Bai, Y. Lin, H. Wei, Zeng, C. Xiao, J. Huang, Defect passivation in hybrid perovskite solar cells using quaternary ammonium halide anions and cations, Nat. Energy 2 (2017) 17102.
[22] T. Liu, K. Chen, Q. Hu, R. Zhu, Q. Gong, Inverted perovskite solar cells: progresses and perspectives, Adv. Energy Mater. 6 (17) (2016) 1600457.
[23] L. Meng, J. You, T.-F. Guo, Y. Yang, Recent advances in the inverted planar structure of perovskite solar cells, Acc. Chem. Res. 49 (1) (2016) 155–165.
[24] J. Seo, S. Park, Y. Chan Kim, N.J. Jeon, J.H. Noh, S.C. Yoon, S.I. Seok, Benefits of very thin PCBM and LiF layers for solution-processed p-i-n perovskite solar cells, Energy Environ. Sci. 7 (8) (2014) 2642–2646.
[25] J.-Y. Jeng, Y.-F. Chiang, M.-H. Lee, S.-R. Peng, T.-F. Guo, P. Chen, T.-C. Wen, CH3NH3PbI3 perovskite/fullerene planar-heterojunction hybrid solar cells, Adv. Mater. 25 (27) (2013) 3727–3732.
[26] J. Xie, X. Yu, X. Sun, J. Huang, Y. Zhang, M. Lei, K. Huang, D. Xu, Z. Tang, C. Cui, D. Yang, Improved performance and air stability of planar perovskite solar cells via interfacial engineering using a fullerene amine interlayer, Nano Energy 28 (2016) 330–337.
[27] H. Zhang, H. Azimi, Y. Hou, T. Ameri, T. Przybilla, E. Spiecker, M. Kraft, U. Scherf, C.J. Brabec, Improved high-efficiency perovskite planar heterojunction solar cells via incorporation of a polyelectrolyte interlayer, Chem. Mater. 26 (18) (2014) 5190–5193.
[28] H. Choi, C.-K. Mai, H.-B. Kim, J. Jeong, S. Song, G.C. Bazan, J.Y. Kim, A.J. Heeger, Conjugated polyelectrolyte hole transport layer for inverted-type perovskite solar cells, Nat. Commun. 6 (2015) 7348.
[29] C.-Y. Chang, Y.-C. Chang, W.-K. Huang, K.-T. Lee, A.-C. Cho, C.-C. Hsu, Enhanced performance and stability of semitransparent perovskite solar cells using solution-processed thiol-functionalized cationic surfactant as cathode buffer layer, Chem. Mater. 27 (20) (2015) 7119–7127.
[30] C.-Y. Chang, W.-K. Huang, J.-L. Wu, Y.-C. Chang, K.-T. Lee, C.-T. Chen, Room-temperature solution-processed n-doped zirconium oxide cathode buffer layer for efficient and stable organic and hybrid perovskite solar cells, Chem. Mater. 28 (1) (2016) 242–251.
[31] Q. Xue, Z. Hu, J. Liu, J. Lin, C. Sun, Z. Chen, C. Duan, J. Wang, C. Liao, W.M. Lau, F. Huang, H.-L. Yip, Y. Cao, Highly efficient fullerene/perovskite planar heterojunction solar cells via cathode modification with an amino-functionalized polymer interlayer, J. Mater. Chem. A 2 (46) (2014) 19598–19603.
[32] Y. Liu, M. Bag, L.A. Renna, Z.A. Page, P. Kim, T. Emrick, D. Venkataraman, T.P. Russell, Understanding interface engineering for high-performance fullerene/perovskite planar heterojunction solar cells, Adv. Energy Mater. 6 (2) (2016) 1501606.
[33] Z. Hu, J. Miao, M. Liu, T. Yang, Y. Liang, O. Goto, H. Meng, Enhanced performance of inverted perovskite solar cells using solution-processed carboxylic potassium salt as cathode buffer layer, Org. Electron. 45 (2017) 97–103.
[34] Q. Wang, C.-C. Chueh, M. Eslamian, A.K.Y. Jen, Modulation of PEDOT:PSS pH for efficient inverted perovskite solar cells with reduced potential loss and enhanced stability, ACS Appl. Mat. Interfaces 8 (2016) 32068–32076.
[35] Q. Wang, C.-C. Chueh, T. Zhao, M. Eslamian, W.C.H. Choy, A.K.Y. Jen, Effects of self-assembling monolayer modification of NiOx nanoparticles layer on the performance of inverted perovskite solar cells and application in high power-per-weight devices, ChemSusChem (2017), http://dx.doi.org/10.1002/cssc.201701262.
[36] V. Biju, P.K. Sudeep, K.G. Thomas, M.V. George, S. Barazzouk, P.V. Kamat, Clusters of bis- and tris-fullerenes, Langmuir 18 (5) (2002) 1831–1839.
[37] M. Qian, M. Li, X.-B. Shi, H. Ma, Z.-K. Wang, L.-S. Liao, Planar perovskite solar cells with 15.75% power conversion efficiency by cathode and anode interfacial modification, J. Mater. Chem. A 3 (25) (2015) 13533–13539.
[38] L.-L. Jiang, S. Cong, Y.-H. Lou, Q.-H. Yi, J.-T. Zhu, H. Ma, G.-F. Zou, Interface engineering toward enhanced efficiency of planar perovskite solar cells, J. Mater. Chem. A 4 (1) (2016) 217–222.
[39] C.-Y. Chang, W.-K. Huang, Y.-C. Chang, Highly-efficient and long-term stable perovskite solar cells enabled by a cross-linkable n-doped hybrid cathode interfacial layer, Chem. Mater. 28 (17) (2016) 6305–6312.
[40] National Center for Biotechnology Information. PubChem Compound Database. CID = 62827, 〈https://pubchem.ncbi.nlm.nih.gov/compound/62827〉 (accessed 26 September 2017).
[41] S. Yue, S. Lu, K. Ren, K. Liu, M. Azam, D. Cao, Z. Wang, Y. Lei, S. Qu, Z. Wang, Insights into the influence of work functions of cathodes on efficiencies of perovskite solar cells, Small 13 (19) (2017) 1700007.
[42] C.-Z. Li, C.-Y. Chang, Y. Zang, H.-X. Ju, C.-C. Chueh, P.-W. Liang, N. Cho, D.S. Ginger, A.K.Y. Jen, Suppressed charge recombination in inverted organic photovoltaics via enhanced charge extraction by using a conductive fullerene electron transport layer, Adv. Mater. 26 (36) (2014) 6262–6267.
[43] C.-Z. Li, C.-C. Chueh, H.-L. Yip, F. Ding, X. Li, A.K.Y. Jen, Solution-processible highly conducting fullerenes, Adv. Mater. 25 (17) (2013) 2457–2461.
[44] C.-Y. Chang, W.-K. Huang, Y.-C. Chang, K.-T. Lee, C.-T. Chen, A solution-processed n-doped fullerene cathode interfacial layer for efficient and stable large-area perovskite solar cells, J. Mater. Chem. A 4 (2) (2016) 640–648.
[45] S.D. Stranks, G.E. Eperon, G. Grancini, C. Menelaou, M.J.P. Alcocer, T. Leijtens, L.M. Herz, A. Petrozza, H.J. Snaith, Electron-hole diffusion lengths exceeding 1 micrometer in an organometal trihalide perovskite absorber, Science 342 (6156) (2013) 341–344.
[46] N.H. Tiep, Z. Ku, H.J. Fan, Recent advances in improving the stability of perovskite solar cells, Adv. Energy Mater. 6 (3) (2016) 1501420.

Zhao Hu grew up in the Hubei province, China. He received his M.S. degree (2013) in Wuhan Institute of Technology. In 2014, he continued his study in Peking University as a Ph.D. candidate. He focuses on the design and synthesis of interfacial materials in organic electronic devices.

Jingsheng Miao received His Ph.D. degree in materials physics from the South China University of Technology, Guangzhou, China in 2015. Afterwards, he joined the School of Advanced Materials in Peking University as a postdoctoral researcher with Prof. Hong Meng. His research interests include perovskite solar cells and organic solar cells.

Tingting Li, currently work as an engineer in the School of Advanced Materials, Peking University, China. Her research interest is morphology studies of organic/inorganic thin films by atomic force microscopy measurement.

Dr. Ming Liu received her Ph.D. from Huazhong University of Science and Technology in Materials in 2014. After her graduation she worked as a Postdoc Researcher with Prof. Hong Meng in Peking University Shenzhen Graduate School until April, 2017. Now she is an research associate and her current research interests are organic-inorganic hybrid solar cells and optoelectronic devices based on quantum dots.

Imran Murtaza, is currently an Assistant Professor of Physics, Research Supervisor approved by Higher Education Commission Pakistan. He worked as a Postdoc at School of advanced materials, Peking University, China. Currently, his research focuses on thin film optoelectronic devices based on organic semiconductors.

Prof. Hong Meng received his Ph.D. from University of California Los Angeles (UCLA) in 2002. He has been working in the field of organic electronics for more than 20 years. His career experiences including working in the Institute of Materials Science and Engineering (IMRE) at Singapore, Lucent Technologies Bell Labs, DuPont Experimental Station. In 2014, he moved to School of Advanced Materials Peking University Shenzhen Graduate School. He has contributed over 90 peer-reviewed papers (citation: 5000) in chemistry and materials science fields, filed over 46 US patents, 50 Chinese patents.